



<http://www.diva-portal.org>

Postprint

This is the accepted version of a paper published in *Nano Energy*. This paper has been peer-reviewed but does not include the final publisher proof-corrections or journal pagination.

Citation for the original published paper (version of record):

Liu, J., Younesi, R., Gustafsson, T., Edström, K., Zhu, J. (2014)
Pt/ α -MnO₂ nanotube: a highly active electrocatalyst for Li-O₂ battery.
Nano Energy, 10: 19-27
<http://dx.doi.org/10.1016/j.nanoen.2014.08.022>

Access to the published version may require subscription.

N.B. When citing this work, cite the original published paper.

Permanent link to this version:

<http://urn.kb.se/resolve?urn=urn:nbn:se:uu:diva-234462>

Pt/ α -MnO₂ nanotube: a highly active electrocatalyst for Li-O₂ battery

*Jia Liu, Reza Younesi, Torbjörn Gustafsson, Kristina Edström, and Jiefang Zhu**

Department of Chemistry-Ångström Laboratory, Uppsala University, Box 538, SE-751 21 Uppsala, Sweden

*Corresponding author. Tel: +46 18 4713722. Fax: +46 18 153548. E-mail: jiefang.zhu@kemi.uu.se

Abstract: The preparation of α -MnO₂ nanotubes (M-NT) decorated with platinum nanoparticles (Pt/M-NT) by a simple reduction and mechanical stirring method is presented in this work, which aims to design a highly active catalyst for the Li-O₂ battery. The obtained samples were characterized by XRD, SEM, TEM, BET, and XPS techniques. The electrocatalytic performance of the prepared samples was evaluated by tracking the decomposition of Li₂O₂ during the charging process in a Li-O₂ cell using *in situ* XRD and *operando* SR-PXD, which gave direct and time resolved information during the whole process. The results indicated that Pt nanoparticles were uniformly dispersed on the surface of M-NT. Even a small amount (1 wt%) of Pt on M-NT did largely enhance the kinetics of the charging process. A cell with 5 wt% Pt/M-NT showed the highest catalytic activity and lowest charging potential. The decomposition of Li₂O₂ during the charging process in a Li-O₂ cell with 5 wt% Pt/M-NT followed a zero-order reaction. This promoting effect from the supported nanocatalyst can be attributed to the high surface area, highly dispersed and uniform Pt deposition, and proper surface state modifications.

Keywords: Pt nanoparticle, MnO₂ nanotube, Li-O₂ battery, charging process, electrocatalysis, *operando* synchrotron-based XRD.

1. Introduction

As an advanced energy storage and conversion system, the rechargeable Li-O₂ battery, firstly presented in 1996, has recently attracted considerable attention because of its high gravimetric density [1, 2]. In an ideal Li-O₂ battery, on discharge, O₂ is reduced at the cathode where it combines with Li⁺ released from the Li-metal anode to yield Li₂O₂ (oxygen reduction reaction (ORR), $2 \text{Li}^+ + \text{O}_2 \uparrow + 2 \text{e}^- \rightarrow \text{Li}_2\text{O}_2$). On charge, Li₂O₂ is converted back to Li⁺ and O₂ (oxygen evolution reaction (OER), $\text{Li}_2\text{O}_2 \rightarrow 2 \text{Li}^+ + \text{O}_2 \uparrow + 2 \text{e}^-$). One of the critical challenges, which limit the application of Li-O₂ batteries, is the low round-trip efficiency resulting from a large overpotential, especially due to the high charging voltage [3, 4]. Although the real role of the catalyst is controversial and the catalytic mechanism is not yet clear [5-7], it has been widely accepted that ORR kinetics in a Li-O₂ battery is catalytically insensitive, since carbon which is used as a porous cathode alone provides a sufficient catalytic promotion [8, 9], while the counterpart OER shows a different situation, i.e. the use of a catalyst seems to lower the charging voltage of Li-O₂ cells [10, 11].

Up to now, a number of materials have been employed as cathode catalysts, such as noble metals (or their alloys) [8, 12, 13], carbonaceous materials [14, 15], and transition-metal oxides [16, 17]. Platinum (Pt) as a highly stable and superior electrocatalytic noble metal has shown to facilitate oxygen evolution and lower the activation barrier in the OER [12, 18, 19]. However, the cost and scarcity of Pt limit its application in Li-O₂ batteries. Since other mono-component catalysts cannot usually compete with precious metal catalysts, attempts have been made to use supported noble metal catalysts. Pt dispersed on supporting materials as heterogeneous catalysts could even exceed the catalytic performance of Pt [20, 21], since the aggregation and/or big size of single-species Pt particles normally decrease its surface area, which can inevitably depress the electrocatalytic activity. In this respect, Pt supported on Co₃O₄ (Pt/Co₃O₄) [22], graphene (Pt/graphene) [23], titanium nitride nanotubes (Pt/TiN) [24], and carbon nitride (Pt/CN) [25] have been reported as catalysts in Li-O₂ batteries.

Manganese oxide (MnO₂) is another effective catalyst in Li-O₂ batteries, and is considered

as the most favorable trade-off between cost and electrocatalytic activity. The catalytic activity depends on the crystal phase, morphology, and surface area of MnO_2 [26]. Thackeray et al. demonstrated that the catalytic activity of MnO_2 in a Li-O_2 battery followed an order of $\alpha > \beta > \gamma$ phase, since α - MnO_2 displayed high electrical conductivity and intrinsic tunnel size [13]. Bruce et al. reported that α - MnO_2 nanowires as a catalyst with an optimized structure delivered a capacity of 3000 mA h g^{-1} based on the carbon mass in the cathode of the Li-O_2 battery [27]. Recently, α - MnO_2 nanotubes showed better catalytic performance than α - MnO_2 nanowires, due to its higher surface area and unique tunnel structure [28]. In addition, MnO_2 can also be used as a catalyst support in Li-O_2 battery. α - MnO_2 decorated with Au and Pd [29], and mesoporous α - MnO_2 coated with Pd [30] have been used as catalysts in Li-O_2 batteries. However, MnO_2 supported Pt catalyst in Li-O_2 battery has not been reported.

There are many factors that can affect the catalytic activity of Pt, such as its synthesis method and the choice of support. Using a nanoscale support is a promising approach to stabilize a nanostructured catalyst with good dispersion, in order to generate synergistic effects. Equally, it has been reported that the implementation of nanosized materials can not only imply a better electronic conductivity but also offer a robust support for cathode catalyst [31]. The morphology of the support can influence the catalytic activity of Pt, as it can affect the Pt particle size, the Pt dispersion, the Pt-support interaction, and the exposure of more reactive planes. In addition, the surface area is also critical for the function of the electrocatalyst and its support [16, 32]. Although α - MnO_2 nanotubes displayed its first sign as a good catalyst [28], it has rarely been used as a catalyst support in Li-O_2 batteries.

Here, we explore a facile route for the synthesis of Pt-deposited α - MnO_2 nanotubes, which is expected to exhibit an excellent electrocatalytic activity in OER. α - MnO_2 nanotubes (M-NT) deposited by various amounts of highly dispersed Pt nanoparticles (Pt/M-NT) were prepared by a simple reduction and mechanical stirring method at a low temperature. The electrocatalytic activity of prepared samples was evaluated by the decomposition of Li_2O_2 during the charging process in a Li-O_2 cell. The effects of the amount of deposited Pt on the kinetic of OER were systematically investigated. In addition, *operando* synchrotron-based

XRD (SR-PXD) as a diagnostic tool that allowed us to probe the degradation of Li_2O_2 was employed to offer a good insight into the real time kinetics of OER in a Li- O_2 cell [33].

2. Experimental

2.1. Preparation of M-NT

All chemicals were analytic grade and used as received without any further purification. M-NT preparation by hydrothermal treatment followed the process [34]: 0.597 g potassium permanganate(VII) (KMnO_4 , Merck) powder was dissolved into 70 mL deionized water. Under vigorous stirring, 1 mL hydrochloric acid (HCl, 37%, Prolabo) was dropwise added to the solution. After stirring for 0.5 h, the resultant hydrothermal precursor was transferred to an autoclave, and maintained at 140 °C for 12 h. After the hydrothermal crystallization, the resulting black product, M-NT, was filtered and washed by deionized water, and then dried at 60 °C for 12 h.

2.2. Preparation of Pt/M-NT

The preparation of x wt% Pt/M-NT (x=0.2, 1, 5, 10) was carried out by a simple reduction and mechanical stirring method. An appropriate volume of 0.4 M sodium borohydride (NaBH_4 , Merck) in 0.025 M NaOH solution was added drop-wise into a 0.1 wt% chloroplatinic acid hexahydrate ($\text{H}_2\text{PtCl}_6 \cdot 6\text{H}_2\text{O}$, Aldrich) aqueous solution under vigorous stirring at 60 °C. After stirring for additional 0.5 h, the reaction mixture was allowed to cool down to the room temperature. 0.1 g as-prepared M-NT was added to the solution and kept under stirring for 24 h. The resultant product was filtered and washed several times with deionized water, and then dried at 60 °C for 12 h. X wt% Pt/M-NT (x=0.2, 1, 5, 10) were obtained by adjusting the dosages of NaBH_4 and $\text{H}_2\text{PtCl}_6 \cdot 6\text{H}_2\text{O}$, according to the theoretical values of raw materials. Commercial Pt (Pt black, Fluka) acted as a benchmark material to compare with the electrocatalytic performance of as-prepared samples.

2.3. Preparation of Li_2O_2 -based electrode and assembly of electrochemical cell

The porous Li_2O_2 -based electrodes were prepared inside an Ar-filled glove box (H_2O and $\text{O}_2 < 1$ ppm). All the electrodes were made with a composition of Super P carbon (lithium

battery grade, Erachem Comilog), Pt/M-NT or Pt catalyst, Kynar 2801 (a copolymer based on PVDF, Arkema), silicon (99.5%, Alfa Aesar), and Li_2O_2 powder (technical grade, 90%, Sigma-Aldrich) in a weight ratio of 40:8:7:10:35. As an inert internal standard, silicon was used as a reference to estimate the amount of Li_2O_2 in the electrode by XRD. Super P carbon, catalyst, silicon, and Li_2O_2 were mixed by high energy ball-milling for 1.5 h. Then, Kynar as a binder and acetone ($\geq 99.0\%$, Fluka) as solvent were added to the mixture to prepare a slurry, which was hand-milled for 0.5 h. The slurries were cast onto an aluminum mesh with the diameter of 1.3 cm. After the acetone evaporated, the electrodes were transferred to a vacuum oven (Buchi Glass Oven B-585) and dried at $120\text{ }^\circ\text{C}$ for 5 h.

The components of all the electrochemical cells were assembled in a "coffee bag" (aluminium pouch cell) type in an Ar-filled glove box (H_2O and $\text{O}_2 \leq 3$ ppm) as the following: Li metal negative electrode, double-layer Solupor separator presoaked in electrolyte (1 M LiPF_6 in propylene carbonate (PC), Ferro, Purolyte), and Li_2O_2 -based positive electrode described above, as shown in Figures S1 (a) and (b) in Supplementary Information (SI).

The battery performance testing was run by using 1 M LiClO_4 in Dimethyl sulfoxide (DMSO) as electrolyte. The experimental details can be found in Supplementary data.

2.4. Electrochemical testing

All the electrochemical cells were charged for 15 h using an external potentiostat (SP-240, Bio-Logic SAS) at a constant current density of $40\text{ mA g}_{\text{Li}_2\text{O}_2}^{-1}$ from open circuit voltage.

2.5. Characterization

The XRD analyses of as-prepared x wt% Pt/M-NT were performed using a Bruker D8 TwinTwin X-ray diffractometer (XRD), operating at 40 kV and 40 mA, using Cu $K\alpha$ radiation ($\lambda=1.5406\text{ \AA}$). In order to compare the electrocatalytic activities of different catalysts, *in situ* XRD analysis (XRD measurement of a whole cell without unpacking it before and after charging) was employed to study the electrochemical decomposition of Li_2O_2 , which was carried out by an in house STOE diffractometer with a position-sensitive detector and Co $K\alpha$ radiation ($\lambda=1.789\text{ \AA}$), operating at 45 kV and 32 mA, in transmission mode. To further study the kinetics of OER, *operando* SR-PXD (operating synchrotron-based

XRD during charging process of a cell) was conducted using the beamline I711 with the wavelength (λ) of 0.993 Å at Max IV Laboratory in Lund, Sweden (Figures S1(b-d) in SI [35]). The cells were mounted in transmission mode, and an Oxford diffraction Titan CCD area detector was used to collect diffraction patterns. Lanthanum hexaoride (LaB₆, SRM-660) acted as a reference for calibrating the different parameters of powder diffraction instrument, such as sample-to-detector distance, wavelength, and detector tilt angle. In our previous work, the electrochemical decomposition of Li₂O₂ was dramatically accelerated under the continuous X-ray irradiation [33]. Therefore, in order to avoid the negative influence of X-ray illumination, data were collected every 30 minute (an exposure time of 20 seconds was used to collect one on the area detector. This frame could later be converted to a plot of intensity vs. 2θ by the program Fit2D). The program FullProf was used to refine the *in situ* XRD and *operando* SR-PXD patterns and analyze the weight fraction of Li₂O₂ and Si ($F_{Li_2O_2}$ and F_{Si}) [36], respectively. The residual ratio of Li₂O₂ (R) in each cell after the charging was calculated from the following formula:

$$R (\%) = \frac{W'_{Li_2O_2}}{W_{Li_2O_2}} \times 100\% = \frac{W'_{Li_2O_2}/W'_{Si}}{W_{Li_2O_2}/W_{Si}} \times 100\% = \frac{\left(\frac{W'_{Li_2O_2}}{W'_{Li_2O_2}+W'_{Si}}\right)/\left(\frac{W'_{Si}}{W'_{Li_2O_2}+W'_{Si}}\right)}{\left(\frac{W_{Li_2O_2}}{W_{Li_2O_2}+W_{Si}}\right)/\left(\frac{W_{Si}}{W_{Li_2O_2}+W_{Si}}\right)} \times 100\% = \frac{F'_{Li_2O_2}/F'_{Si}}{F_{Li_2O_2}/F_{Si}} \times 100\% \quad (1)$$

in which $F_{Li_2O_2}$, F_{Si} , $W_{Li_2O_2}$, W_{Si} , $F'_{Li_2O_2}$, F'_{Si} , $W'_{Li_2O_2}$, and W'_{Si} are the weight fraction of Li₂O₂ and Si, and the weight of Li₂O₂ and Si before and after charging, respectively.

The BET surface area and porosity of the obtained samples were determined by a nitrogen adsorption apparatus (Micromeritics ASAP 2020). The morphology, particle size and elements analyses of samples were examined by scanning electron microscopy coupled with energy dispersive spectroscopy (SEM/EDS-Zeiss 1550 with Aztec EDS). Detailed particle and crystal information was obtained by high resolution transmission electron microscopy (HRTEM Tecnai F30), operating at an accelerating voltage of 300 kV. X-ray photoelectron spectroscopy (XPS) measurement was employed to study the surface composition and chemical states of as-prepared samples by a Perkin Elmer PHI 5500 system using Al K α

radiation ($h\nu=1486.7$ eV) and an emission angle of 45° . The binding energy scale was calibrated using C 1s peak assigned to the C-H bond at 285 eV.

3. Results and Discussion

Table 1. Characteristics of as-prepared x wt% Pt/M-NT ($x=0, 1, 5, 10$)

sample	x wt% Pt/M-NT			crystallite size of Pt from XRD (nm)	particle size of Pt from TEM (nm)	S_{BET} (m^2/g)
	calculated x	x obtained by EDS	x obtained by XPS			
M-NT	0	0	0	-	-	17.11
1 wt% Pt/M-NT	1	0.8	3.7	-	6.89	17.37
5 wt% Pt/M-NT	5	4.5	19.7	11.1	7.11	19.36
10 wt% Pt/M-NT	10	10.3	31.1	11.7	7.12	20.56

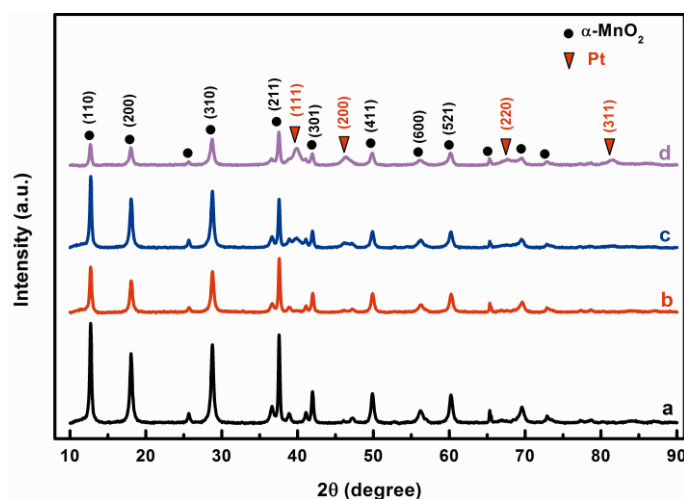


Figure 1. XRD patterns of (a) M-NT, (b) 1 wt% Pt/M-NT, (c) 5 wt% Pt/M-NT, and (d) 10 wt% Pt/M-NT.

The XRD analysis of as prepared x wt% Pt/M-NT ($x=0, 1, 5, 10$) was conducted for the phase identification. The main peaks of XRD patterns of all the samples at $2\theta=12.7^\circ, 18.1^\circ, 28.7^\circ$, and 37.5° (see Figure 1) could be perfectly indexed to the tetragonal phase of α - MnO_2 (JCPDS Card No. 04-007-2142). No characteristic peak corresponding to Pt in 1 wt% Pt/M-NT was observed due to the low content of deposited Pt. However, for 5 wt% Pt/M-NT and 10 wt% Pt/M-NT, the peaks at $2\theta=39.7^\circ, 46.2^\circ, 67.7^\circ$, and 81.6° corresponding to (111), (200), (220), and (311) planes of Pt (JCPDS Card No. 01-087-0640) were presented in the pattern,

respectively. The crystallite sizes of Pt were estimated by Scherrer's formula using the full width at half maximum of the most intense Pt peak (111). As presented in Table 1, the crystallite size of Pt deposited on 5 wt% Pt/M-NT and 10 wt% Pt/M-NT was 11.1 nm and 11.7 nm, respectively.

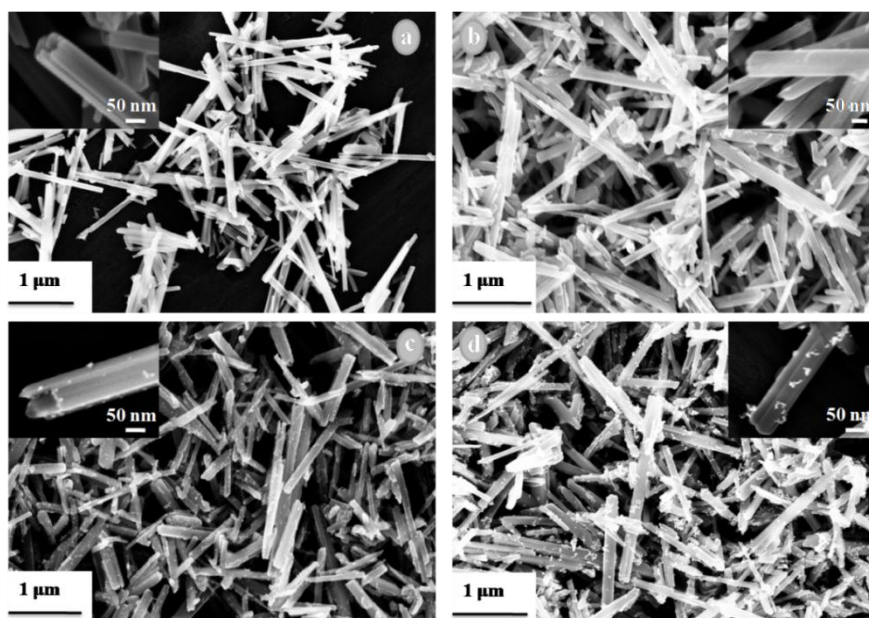


Figure 2. SEM images of (a) M-NT, (b) 1 wt% Pt/ M-NT, (c) 5 wt% Pt/ M-NT, and (d) 10 wt% Pt/ M-NT.

Figure 2 presents SEM images of as prepared x wt% Pt/M-NT ($x=0, 1, 5, 10$). It can be seen that M-NTs showed uniform “tube-like” shapes and smooth surfaces (Figure 2(a)). All Pt deposited samples displayed a similar morphology and particle size of M-NT, which were not affected by Pt loading (Figures 2(b-d)). Pt particles were highly dispersed and attached on to the surfaces of M-NT as shown in Figure 2(b) and Figure 2(c). However, 10 wt% Pt/M-NT showed some visible agglomeration of Pt particles (Figure 2(d)). To investigate the chemical composition of as-synthesized samples, EDS analysis was employed and the results are shown in Table 1. The contents of Pt in the final x wt% Pt/M-NT samples obtained from EDS analysis were in good accordance with the values calculated from their syntheses, which indicated that the synthesis of the different Pt/M-NT samples from a simple reduction and mechanical stirring method is reliable and controllable. Detailed particle and crystal information were obtained by TEM and HRTEM (See Figures S2, S3 in SI and Table 1).

The BET surface areas of as prepared x wt% Pt/M-NT (x=0, 1, 5, 10) are presented in Table 1. It is noted that the BET surface areas gradually increased from 17.10 to 20.56 m² g⁻¹ with the increasing content of Pt, from M-NT to 10 wt% Pt/ M-NT. **This indicates that the highly dispersed Pt nanoparticles contributed to a slight increase of the surface area, which is beneficial to the catalytic performance.** The sample 5 wt% Pt/M-NT had a pore size distribution in the range of 10-150 nm (Figure S4 in SI).

Table 2. Binding energy of XPS spectra of M-NT and 5 wt% Pt/M-NT samples and relative contribution of each peak to deconvoluted O1s spectra.

sample	binding energy (eV)					O _L (%)	O _H (%)	O _H /O _L
	Mn2p _{3/2}	Pt4f _{7/2}	O _L 1s (M-O)	O _H 1s (O-H)	O-C-O			
M-NT	642.5	-	530	531.5	533.2	78.7	16.7	21.2
5 wt% Pt/M-NT	642.3	71.7, 72.8, and 74.7	529.9	531.4	533.2	74.6	19.7	26.4

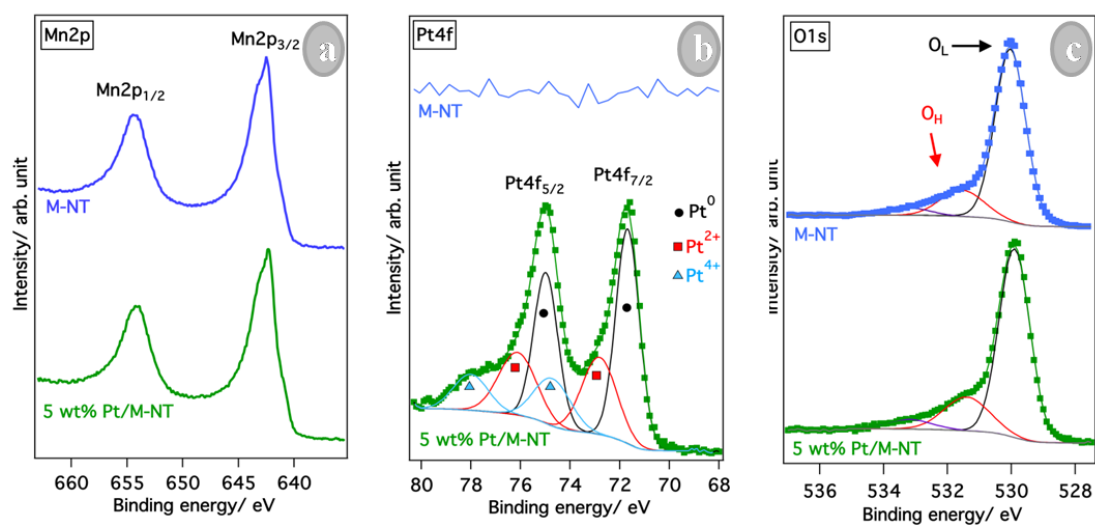


Figure 3. XPS core level spectra of (a) Mn2p, (b) Pt4f and its curve fitting, and (c) O1s and its curve fitting for the M-NT and 5 wt% Pt/M-NT samples.

To further study the chemical states and surface composition of the Pt-deposited α -MnO₂, two representative samples M-NT and 5 wt% Pt/M-NT were characterized by XPS (Figure 3). The Mn2p spectra of M-NT and 5 wt% Pt/M-NT depicted in Figure 3a contain two peaks at 642.6 and 654.2 eV with the spin-orbit separation of 11.6 eV, which were in good accordance with the binding energy of Mn2p_{3/2} and Mn2p_{1/2}, respectively, indicating that the Mn element mainly existed as a chemical state of Mn⁴⁺ [37]. **The Pt4f spectrum of the 5 wt% Pt/M-NT**

sample reveals the presence of Pt in at least three different charge states at binding energies of 71.7, 72.8, and 74.7 eV ($Pt4f_{7/2}$), respectively, with their spin-orbit split doublets ($Pt4f_{5/2}$) at 3.3 eV higher binding energy for each peak. The first peak at 71.7 eV, which has the main contribution to the spectrum, indicates the major existence of Pt as Pt^0 [38]. The second and third peaks at 72.8 and 74.7 eV represent Pt^{2+} and Pt^{4+} , respectively [38]. The relative amounts of Pt in the different x wt% Pt/M-NT samples obtained from XPS measurements are given in Table 1. Generally, XPS results provide the composition of the very surface of the as-prepared samples, while EDS analysis reflect the deep and average composition. The values obtained from XPS were much higher (about 4 times) than those obtained from EDS and calculated from the synthesis process, indicating that Pt nanocrystals were highly distributed on the surfaces of obtained samples. This can explain why even 1 wt% Pt/M-NT can show considerable catalytic activity, since catalysis is a surface process. The O1s spectra of these two samples in Figure 3c are asymmetric, indicating that there should be at least more than one chemical form present. The deconvolution of the 5 wt% Pt/M-NT sample shows the main contribution at binding energy of 529.9 eV corresponding to oxygen in the MnO_2 lattice (O_L). The second one at 531.4 eV corresponds to oxygen from chemisorbed H_2O (O_H) on the MnO_2 surface, and the third peak at 533.2 eV presents oxygen from a small contamination containing ether bonds (O-C-O) (Figure 3c and Table 2). The binding energies of XPS spectra and relative contribution of peaks to O1s spectra are listed in Table 2. As seen in Table 2, the amount of surface hydroxyl oxygen in 5 wt% Pt/M-NT is higher than that of M-NT, which may result from the increment of surface oxygen vacancies by Pt decoration. As a very active group, the oxygen vacancies can easily combine with water absorbed on the surface of sample to form surface hydroxyl oxygen [39, 40]. Rossmeislet al. demonstrated by DFT calculations that increasing surface hydroxyl oxygen and oxygen vacancies could be favorable to the oxygen evolution reaction [41]. Therefore, 5 wt% Pt/M-NT, compared to M-NT, is expected to show better catalytic activity, due to its proper surface state modifications.

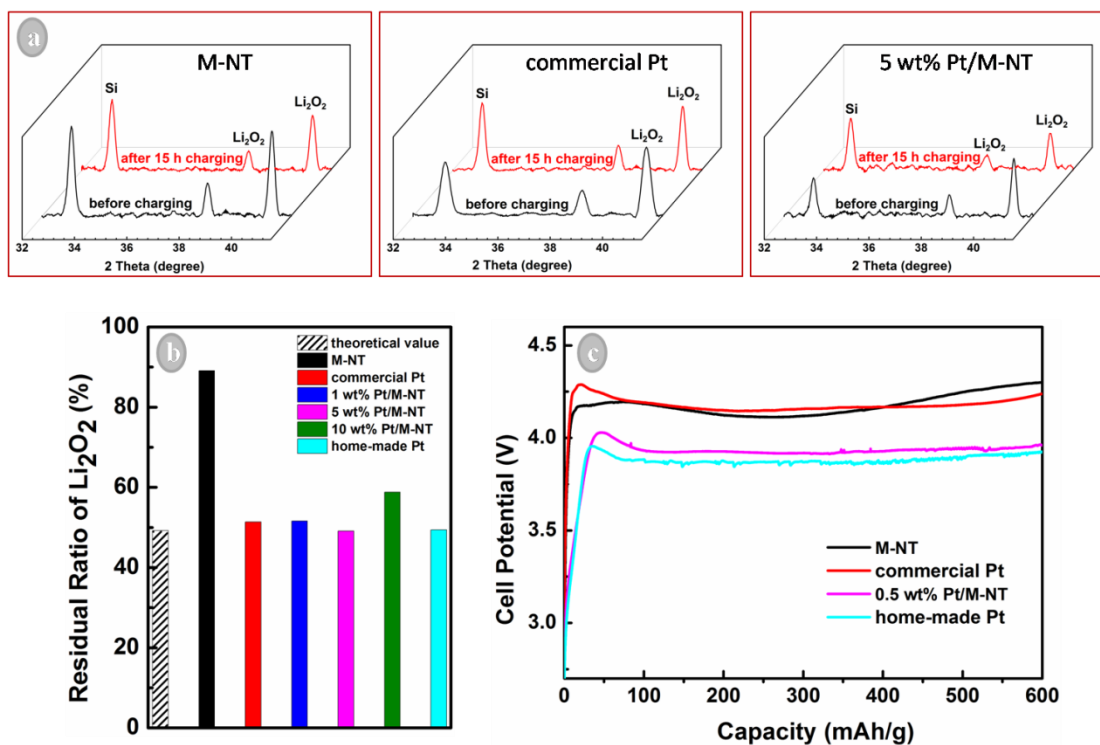


Figure 4. (a) The *in situ* XRD patterns of Li₂O₂-based electrodes with three representative samples (M-NT, commercial Pt, and 5 wt% Pt/M-NT) before and after charging for 15 h at a constant current of 40 mA g_{Li₂O₂}⁻¹, (b) the residual ratios of Li₂O₂ in the electrodes with different catalysts after 15 h of charging, and (c) charging curves of the cells with four representative catalysts (M-NT, commercial Pt, home-made Pt, and 5 wt% Pt/M-NT) charged for 15 h.

In the Li-O₂ cells, we used 1 M LiPF₆ in PC as electrolyte to study charging process. Although PC has proved to be decomposed by the intermediate superoxide species (O₂⁻) formed during the discharge reaction (ORR) in a Li-O₂ battery [42, 43], we chose PC as the electrolyte solvent for this study because: i) it has successfully been used to analyze the oxidation of Li₂O₂ in a cell assembled at the discharge state (i.e. studying only OER) [13, 33, 44]; and ii) the oxidation potential of PC solvent is higher than that of ether [5]. It becomes hence a model system for studying catalytic activity of x wt% Pt/M-NT samples.

In order to scrutinize the contribution of each component in the catalyst composites, we also synthesized pure Pt nanoparticles in the same synthetic condition (home-made Pt nanoparticles) for comparison. X wt% Pt/M-NT, commercial and home-made Pt were used as catalysts in the cathodes of Li-O₂ cell, and their performances were evaluated by tracking the decomposition of Li₂O₂ in cells charged for 15 h at a constant current density of 40 mA g_{Li₂O₂}⁻¹.

The *in situ* XRD patterns of Li_2O_2 -based electrodes with three representative samples M-NT, commercial Pt, and 5 wt% Pt/M-NT before and after charging for 15 h are shown in Figure 4(a). $\alpha\text{-MnO}_2$ was believed to be a promising bifunctional (for both ORR and OER) catalyst for Li-O₂ battery, because Li^+ intercalation into its special 2×2 channel of tunnel frame structure could create an positive environment on the surface which is favorable for the formation of oxygen-rich surfaces in Li_2O_2 with lower OER potential [13, 45, 46]. However, as shown in Figure 4(b), there existed a significant difference between the residual ratio of Li_2O_2 in the electrode with M-NT catalyst (89%) and the calculated theoretical value (49.2%) from the charging capacity of the cell, indicating that OER cannot be promoted by only M-NT itself. These values reveal that the charging process of a Li-O₂ cell with M-NT catalyst is accompanied with considerable amounts of parasitic reactions. The residual ratio of Li_2O_2 in the electrode with 0.2 wt% Pt/M-NT, 1 wt% Pt/M-NT, 5 wt% Pt/M-NT, and 10 wt% Pt/M-NT decreased to 75%, 52%, 49%, and 59%, respectively, as compared to those of commercial Pt (51%) and home-made Pt (49.4%). From these results, it can be well established that a small amount of Pt decoration on M-NT did largely enhance the kinetics of OER. **The residual ratio (49%) of Li_2O_2 in the electrode with 5 wt% Pt/M-NT after 15 h of charging is close to those in the electrode with commercial Pt (51%) and home-made Pt (49.4%), further indicating that 5 wt% decoration by Pt nanoparticles on M-NT was enough to enhance the charging efficiency in a Li-O₂ cell.** Regarding the catalytic activity for the decomposition of Li_2O_2 , 5 wt% Pt/M-NT showed maximum activity due to its higher surface area, highly dispersed and uniform Pt deposition, and proper surface state modifications. Moreover, the residual ratio of Li_2O_2 (49%) in the electrode with 5 wt% Pt/M-NT after 15 h of charging agreed well with the calculated theoretical value (49.2%), indicating that Li_2O_2 decomposition is the main reaction during OER in this cell. In other words, appropriate Pt decoration on M-NT could suppress the side reactions (e.g. electrolyte decomposition) during the charging process of a Li-O₂ cell. Figure 4(c) shows the charging curves of the cells with four representative catalysts (M-NT, commercial Pt, home-made Pt nanoparticles, and 5 wt% Pt/M-NT), which indicates that M-NT decorated by Pt nanoparticles could lower the charging

potential, compared to commercial Pt and un-decorated M-NT. No significant difference between the charging profiles of the cells with home-made Pt and 5 wt% Pt/M-NT was observed.

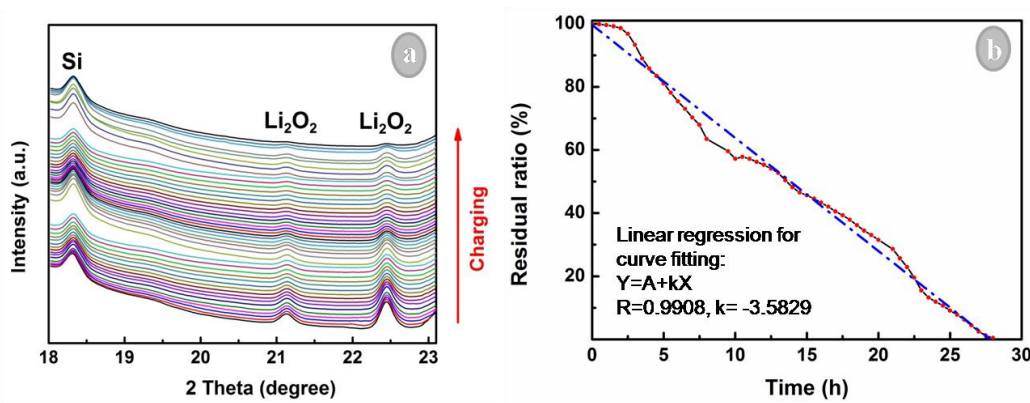


Figure 5.(a) The *operando* SR-PXD patterns of an electrode using the sample 5 wt% Pt/M-NT as catalyst collected every 30 min during charging for 27.5 h, and (b) the curve (—) and linear curve fitting (---) of Li_2O_2 decomposition during the *operando* SR-PXD test.

To further study the kinetics of the charging process in the catalyst-based system, *operando* SR-PXD was employed to track the decomposition of Li_2O_2 . Figure 5(a) shows the *operando* SR-PXD patterns of an electrode with 5 wt% Pt/M-NT sample collected during the charging process at a constant current of $40 \text{ mA g}_{\text{Li}_2\text{O}_2}^{-1}$. Li_2O_2 (JCPDS File No: 04-013-3506) and Si (JCPDS File No: 04-014-0211) crystal phases were observed. The change in the absolute intensity of the Si reference peak was attributed to the injection of synchrotron beam (as the intensity of synchrotron beam gradually faded during measurement). Almost all Li_2O_2 is decomposed after 27.5 h of charging (Figure 5(b)), which is a small difference compared with the theoretical value (29.5 h) calculated from the charging capacity. This could be attributed to the low resolution for the small amount of Li_2O_2 left at the final stage of charging, and/or the effect of X-ray acceleration on Li_2O_2 decomposition [33]. Since the Li_2O_2 decomposition occurs approximately linearly with respect to time, as seen in Figure 5(b), *pseudo-zero-order* kinetics was assumed to evaluate the corresponding decomposition rate constant k :

$$R'_{\text{Li}_2\text{O}_2} = R_{\text{Li}_2\text{O}_2} - kt \quad (2)$$

Where $R_{\text{Li}_2\text{O}_2}$ and $R'_{\text{Li}_2\text{O}_2}$ are the residual ratio of Li_2O_2 before charging, and during the

charging time t (h), respectively, and k (h^{-1}) is the zero-order decomposition rate constant. From the results obtained from curve fitting, the decomposition of Li_2O_2 in a cell with the 5 wt% Pt/M-NT catalyst followed a zero-order reaction, and the decomposition rate constant is 3.5829 h^{-1} . This value is close to the ideal decomposition rate constant of charging process in a Li- O_2 cell, indicating that there are very minor parasitic reactions with 5 wt% Pt/M-NT.

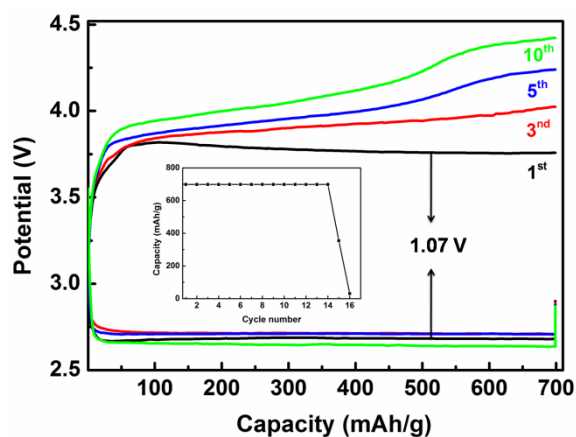


Figure 6. The discharge-charge profile of Li- O_2 cells with 5 wt% Pt/M-NT at a constant current density of $70 \text{ mA g}_{\text{carbon}}^{-1}$, using 1 M LiClO_4 in DMSO electrolyte. Inset: Delivered discharge capacity vs cycle number. The experimental details can be seen in Supplementary data.

Figure 6 shows the discharge-charge curves of a Li- O_2 cell with 5 wt% Pt/M-NT using a current density of $70 \text{ mA g}_{\text{carbon}}^{-1}$. (Cyclability of Li- O_2 cells at different current densities is shown in Figure S5 and S6 in SI). Since PC easily decomposes in ORR [42], we used dimethyl sulfoxide (DMSO) as the electrolyte solvent, which is considered as one of the most stable solvents for ORR in Li- O_2 cells, even though it degrades partially [47, 48]. The cell displayed overpotential of 1.07 V in the first cycle, which increased gradually with the cycle number due to the raising of charge potential. The inset in Figure 6 shows that the discharge capacity was dropped after 14 cycles. Besides the fact that DMSO is not completely stable in Li- O_2 cells [47, 48], instability of Li metal anode in contact with DMSO is another reason for the sudden death of the cells [49]. Further studies to elucidate the influence of catalysts on ORR require a truly stable electrolyte to avoid parasitic reactions. However, for the time being the role of catalysts in the electrochemical decomposition of Li_2O_2 can be investigated using the model system with a PC-based electrolyte presented in this work.

4. Conclusion

α -MnO₂ nanotubes decorated with x wt% Pt (x=0, 0.2, 1, 5, 10) were successfully synthesized by a simple reduction and mechanical stirring method at a low temperature. The conclusions obtained are: (i) from the sample composition analysis, the preparation of the supported catalysts is reliable and controllable; (ii) Pt nanoparticles were dispersed uniformly on the surface of M-NT, and the loaded Pt did not affect the morphology and size of M-NT; (iii) the BET surface areas gradually increased with the increasing content of Pt; (iv) a small amount of decoration by Pt on M-NT did largely enhance the efficiency and selectivity of charging process in a Li-O₂ cell; (v) 5 wt% Pt/M-NT showed the highest catalytic activity due to its higher surface area, highly dispersed and uniform Pt deposition, and proper surface state modifications; and (vi) the decomposition of Li₂O₂ with 5 wt% Pt/M-NT catalyst during the charging process in a Li-O₂ cell followed a zero-order reaction, virtually without any side reactions, confirmed by tracking decomposition of Li₂O₂ using *in situ* XRD and *operando* SR-PXD.

Acknowledgements

This work is financially supported by Swedish Research Council, Swedish Energy Agency, Ångpanneföreningen's Foundation for Research and Development, and J. Gust. Richert Foundation. We thank MAX IV Laboratory for the support of the synchrotron radiation powder XRD measurement. Cuiyan Li is gratefully acknowledged for the TEM measurement.

Reference:

- [1] Y. Shao, F. Ding, J. Xiao, J. Zhang, W. Xu, S. Park, J.-G. Zhang, Y. Wang, J. Liu, Making Li-Air Batteries Rechargeable: Material Challenges, *Advanced Functional Materials*, 23 (2013) 987-1004.
- [2] P.G. Bruce, S.A. Freunberger, L.J. Hardwick, J.M. Tarascon, Li-O₂ and Li-S batteries with high energy storage, *Nature materials*, 11 (2012) 19-29.
- [3] J.-S. Lee, S. Tai Kim, R. Cao, N.-S. Choi, M. Liu, K.T. Lee, J. Cho, Metal-air batteries with high energy density: Li-air versus Zn-air, *Advanced Energy Materials*, 1 (2011) 34-50.
- [4] Y.-C. Lu, B.M. Gallant, D.G. Kwabi, J.R. Harding, R.R. Mitchell, M.S. Whittingham, Y. Shao-Horn, Lithium-oxygen batteries: bridging mechanistic understanding and battery performance, *Energy & Environmental Science*, 6 (2013) 750-768.

- [5] B.D. McCloskey, D.S. Bethune, R.M. Shelby, G. Girishkumar, A.C. Luntz, Solvents' critical role in nonaqueous lithium-oxygen battery electrochemistry, *The Journal of Physical Chemistry Letters*, 2 (2011) 1161-1166.
- [6] Y.-C. Lu, H.A. Gasteiger, Y. Shao-Horn, Catalytic activity trends of oxygen reduction reaction for nonaqueous Li-air batteries, *Journal of the American Chemical Society*, 133 (2011) 19048-19051.
- [7] B.D. McCloskey, R. Scheffler, A. Speidel, D.S. Bethune, R.M. Shelby, A.C. Luntz, On the efficacy of electrocatalysis in nonaqueous Li-O₂ batteries, *J Am Chem Soc*, 133 (2011) 18038-18041.
- [8] Y.S.J. Hun-Gi Jung, Jin-Bum Park, Yang-Kook Sun, Bruno Scrosati, and Yun Jung Lee, Ruthenium-based electrocatalysts supported on reduced graphene oxide for lithium-air Batteries, *ACS Nano*, 7 3532-3539.
- [9] F. Li, T. Zhang, H. Zhou, Challenges of non-aqueous Li-O₂ batteries: electrolytes, catalysts, and anodes, *Energy & Environmental Science*, 6 (2013) 1125-1141.
- [10] Y.-C. Lu, H.A. Gasteiger, M.C. Parent, V. Chiloyan, Y. Shao-Horn, The influence of catalysts on discharge and charge voltages of rechargeable Li-oxygen batteries, *Electrochemical and Solid-State Letters*, 13 (2010) A69-A72.
- [11] K.P.C. Yao, Y.-C. Lu, C.V. Amanchukwu, D.G. Kwabi, M. Risch, J. Zhou, A. Grimaud, P.T. Hammond, F. Barde, Y. Shao-Horn, The influence of transition metal oxides on the kinetics of Li₂O₂ oxidation in Li-O₂ batteries: high activity of chromium oxides, *Physical Chemistry Chemical Physics*, 16 (2014) 2297-2304.
- [12] Y.-C. Lu, Z. Xu, H.A. Gasteiger, S. Chen, K. Hamad-Schifferli, Y. Shao-Horn, Platinum-Gold nanoparticles: A highly active bifunctional electrocatalyst for rechargeable lithium-air batteries, *Journal of the American Chemical Society*, 132 (2010) 12170-12171.
- [13] L. Trahey, N.K. Karan, M.K.Y. Chan, J. Lu, Y. Ren, J. Greeley, M. Balasubramanian, A.K. Burrell, L.A. Curtiss, M.M. Thackeray, Synthesis, characterization, and structural modeling of high-capacity, dual functioning MnO₂ electrode/electrocatalysts for Li-O₂ cells, *Advanced Energy Materials*, 3 (2013) 75-84.
- [14] Z.-L. Wang, D. Xu, J.-J. Xu, L.-L. Zhang, X.-B. Zhang, Graphene oxide gel-derived, free-standing, hierarchically porous carbon for high-capacity and high-rate rechargeable Li-O₂ batteries, *Advanced Functional Materials*, 22 (2012) 3699-3705.
- [15] L. Wang, M. Ara, K. Wadumesthrige, S. Salley, K.Y.S. Ng, Graphene nanosheet supported bifunctional catalyst for high cycle life Li-air batteries, *Journal of Power Sources*, 234 (2013) 8-15.
- [16] Y. Qin, J. Lu, P. Du, Z. Chen, Y. Ren, T. Wu, J.T. Miller, J. Wen, D.J. Miller, Z. Zhang, K. Amine, In situ fabrication of porous-carbon-supported α -MnO₂ nanorods at room temperature: application for rechargeable Li-O₂ batteries, *Energy & Environmental Science*, 6 (2013) 519-531.
- [17] H. Wang, Y. Yang, Y. Liang, G. Zheng, Y. Li, Y. Cui, H. Dai, Rechargeable Li-O₂ batteries with a covalently coupled MnCo₂O₄-graphene hybrid as an oxygen cathode catalyst, *Energy & Environmental Science*, 5 (2012) 7931.
- [18] C.J. Barile, A.A. Gewirth, Investigating the Li-O₂ Battery in an Ether-Based Electrolyte Using Differential Electrochemical Mass Spectrometry, *Journal of the Electrochemical Society*, 160 (2013) A549-A552.
- [19] J. Wang, Y. Li, X. Sun, Challenges and opportunities of nanostructured materials for aprotic rechargeable lithium-air batteries, *Nano Energy*, 2 (2013) 443-467.
- [20] F. Xiao, Y. Li, X. Zan, K. Liao, R. Xu, H. Duan, Growth of metal-metal oxide nanostructures on freestanding graphene paper for flexible biosensors, *Advanced Functional Materials*, 22 (2012) 2487-2494.
- [21] C. Zhou, H. Wang, F. Peng, J. Liang, H. Yu, J. Yang, MnO₂/CNT supported Pt and PtRu nanocatalysts for direct methanol fuel cells, *Langmuir : the ACS journal of surfaces and colloids*, 25 (2009) 7711-7717.
- [22] G. Zhao, J. Lv, Z. Xu, L. Zhang, K. Sun, Carbon and binder free rechargeable Li-O₂ battery cathode with Pt/Co₃O₄ flake arrays as catalyst, *Journal of Power Sources*, 248 (2014) 1270-1274.
- [23] Y. Yang, M. Shi, Q.-F. Zhou, Y.-S. Li, Z.-W. Fu, Platinum nanoparticle-graphene hybrids synthesized by liquid phase pulsed laser ablation as cathode catalysts for Li-air batteries, *Electrochemistry Communications*, 20 (2012) 11-14.
- [24] S. Dong, X. Chen, S. Wang, L. Gu, L. Zhang, X. Wang, X. Zhou, Z. Liu, P. Han, Y. Duan, H. Xu, J. Yao, C. Zhang, K. Zhang, G. Cui, L. Chen, 1D coaxial platinum/titanium nitride nanotube arrays with enhanced electrocatalytic activity for the oxygen reduction reaction: towards Li-air batteries, *ChemSusChem*, 5 (2012) 1712-1715.
- [25] Y. Lu, Z. Wen, J. Jin, Y. Cui, M. Wu, S. Sun, Mesoporous carbon nitride loaded with Pt nanoparticles as a bifunctional air electrode for rechargeable lithium-air battery, *Journal of Solid State Electrochemistry*, 16 (2012) 1863-1868.

- [26] Y. Shao, S. Park, J. Xiao, J.-G. Zhang, Y. Wang, J. Liu, Electrocatalysts for nonaqueous lithium-air batteries: Status, challenges, and perspective, *ACS Catalysis*, 2 (2012) 844-857.
- [27] A. Debart, A.J. Paterson, J. Bao, P.G. Bruce, Alpha-MnO₂ nanowires: a catalyst for the O₂ electrode in rechargeable lithium batteries, *Angewandte Chemie*, 47 (2008) 4521-4524.
- [28] T.T. Truong, Y. Liu, Y. Ren, L. Trahey, Y. Sun, Morphological and Crystalline Evolution of Nanostructured MnO₂ and Its Application in Lithium-Air Batteries, *ACS Nano*, 6 (2012) 8067-8077.
- [29] K.-N. Jung, A. Riaz, S.-B. Lee, T.-H. Lim, S.-J. Park, R.-H. Song, S. Yoon, K.-H. Shin, J.-W. Lee, Urchin-like α -MnO₂ decorated with Au and Pd as a bi-functional catalyst for rechargeable lithium-oxygen batteries, *Journal of Power Sources*, 244 (2013) 328-335.
- [30] A.K. Thapa, T. Ishihara, Mesoporous α -MnO₂/Pd catalyst air electrode for rechargeable lithium-air battery, *Journal of Power Sources*, 196 (2011) 7016-7020.
- [31] A. Kraytsberg, Y. Ein-Eli, The impact of nano-scaled materials on advanced metal-air battery systems, *Nano Energy*, 2 (2013) 468-480.
- [32] J. Wu, H.W. Park, A. Yu, D. Higgins, Z. Chen, Facile synthesis and evaluation of nanofibrous iron-carbon based non-precious oxygen reduction reaction catalysts for Li-O₂ battery applications, *The Journal of Physical Chemistry C*, 116 (2012) 9427-9432.
- [33] J. Liu, M. Roberts, R. Younesi, M. Dahbi, K. Edström, T. Gustafsson, J. Zhu, Accelerated Electrochemical Decomposition of Li₂O₂ under X-ray Illumination, *The Journal of Physical Chemistry Letters*, 4 (2013) 4045-4050.
- [34] J. Luo, H.T. Zhu, H.M. Fan, J.K. Liang, H.L. Shi, G.H. Rao, J.B. Li, Z.M. Du, Z.X. Shen, Synthesis of Single-Crystal Tetragonal α -MnO₂ Nanotubes, *The Journal of Physical Chemistry C*, 112 (2008) 12594-12598.
- [35] Y. Cerenius, K. Ståhl, L.A. Svensson, T. Ursby, Å. Oskarsson, J. Albertsson, A. Liljas, The crystallography beamline I711 at MAX II, *Journal of Synchrotron Radiation*, 7 (2000) 203-208.
- [36] J. Rodríguez-Carvajal, Recent advances in magnetic structure determination by neutron powder diffraction, *Physica B: Condensed Matter*, 192 (1993) 55-69.
- [37] R. Younesi, M. Hahlin, F. Björefors, P. Johansson, K. Edström, Li-O₂ Battery Degradation by Lithium Peroxide (Li₂O₂): A Model Study, *Chemistry of Materials*, 25 (2012) 77-84.
- [38] J.B. Xu, T.S. Zhao, Z.X. Liang, Synthesis of Active Platinum-Silver Alloy Electrocatalyst toward the Formic Acid Oxidation Reaction, *The Journal of Physical Chemistry C*, 112 (2008) 17362-17367.
- [39] J. Liu, Y. Zhao, L. Shi, S. Yuan, J. Fang, Z. Wang, M. Zhang, Solvothermal synthesis of crystalline phase and shape controlled Sn(4+)-doped TiO₂ nanocrystals: effects of reaction solvent, *ACS applied materials & interfaces*, 3 (2011) 1261-1268.
- [40] Q. Ye, J. Zhao, F. Huo, D. Wang, S. Cheng, T. Kang, H. Dai, Nanosized Au supported on three-dimensionally ordered mesoporous β -MnO₂: Highly active catalysts for the low-temperature oxidation of carbon monoxide, benzene, and toluene, *Microporous and Mesoporous Materials*, 172 (2013) 20-29.
- [41] J. Rossmesl, A. Logadottir, J.K. Nørskov, Electrolysis of water on (oxidized) metal surfaces, *Chemical Physics*, 319 (2005) 178-184.
- [42] R. Younesi, S. Urbonaitė, K. Edström, M. Hahlin, The cathode surface composition of a cycled Li-O₂ battery: A photoelectron spectroscopy study, *The Journal of Physical Chemistry C*, 116 (2012) 20673-20680.
- [43] R. Younesi, M. Hahlin, K. Edström, Surface characterization of the carbon cathode and the lithium anode of Li-O₂ batteries using LiClO₄ or LiBOB salts, *ACS applied materials & interfaces*, 5 (2013) 1333-1341.
- [44] W. Xu, K. Xu, V.V. Viswanathan, S.A. Towne, J.S. Hardy, J. Xiao, Z. Nie, D. Hu, D. Wang, J.-G. Zhang, Reaction mechanisms for the limited reversibility of Li-O₂ chemistry in organic carbonate electrolytes, *Journal of Power Sources*, 196 (2011) 9631-9639.
- [45] Y. Cao, Z. Wei, J. He, J. Zang, Q. Zhang, M. Zheng, Q. Dong, [small alpha]-MnO₂ nanorods grown in situ on graphene as catalysts for Li-O₂ batteries with excellent electrochemical performance, *Energy & Environmental Science*, 5 (2012) 9765-9768.
- [46] Y. Mo, S.P. Ong, G. Ceder, First-principles study of the oxygen evolution reaction of lithium peroxide in the lithium-air battery, *Physical Review B*, 84 (2011).
- [47] R. Younesi, P. Norby, T. Vegge, A New Look at the Stability of Dimethyl Sulfoxide and Acetonitrile in Li-O₂ Batteries, *ECS Electrochemistry Letters*, 3 (2014) A15-A18.
- [48] F. Barde, Y. Chen, L. Johnson, S. Schaltin, J. Fransaer, P.G. Bruce, Sulfone Based Electrolytes for Non-Aqueous Li-O₂ Batteries, *The Journal of Physical Chemistry C*, (2014).
- [49] M. Roberts, R. Younesi, W. Richardson, J. Liu, T. Gustafsson, J. Zhu, K. Edström, Increased Cycling Efficiency of Lithium Anodes in Dimethyl Sulfoxide Electrolytes For Use in Li-O₂ Batteries, *ECS Electrochemistry Letters*, 3 (2014) A62-A65.